

# The Influence of Boundary Layer Mixing Strength on the Evolution of a Baroclinic Cyclone

MATTHEW T. VAUGHAN<sup>a</sup> AND ROBERT G. FOVELL<sup>a</sup>

<sup>a</sup>*Department of Atmospheric and Environmental Sciences, University at Albany, State University of New York, Albany, New York*

(Manuscript received 14 August 2020, in final form 1 December 2020)

**ABSTRACT:** Subgrid-scale turbulence in numerical weather prediction models is typically handled by a PBL parameterization. These schemes attempt to represent turbulent mixing processes occurring below the resolvable scale of the model grid in the vertical direction, and they act upon temperature, moisture, and momentum within the boundary layer. This study varies the PBL mixing strength within 4-km WRF simulations of a 26–29 January 2015 snowstorm to assess the sensitivity of baroclinic cyclones to eddy diffusivity intensity. The bulk critical Richardson number for unstable regimes is varied between 0.0 and 0.25 within the YSU PBL scheme as a way of directly altering the depth and magnitude of subgrid-scale turbulent mixing. Results suggest that varying the bulk critical Richardson number is similar to selecting a different PBL parameterization. Differences in boundary layer moisture availability, arising from reduced entrainment of dry, free tropospheric air, lead to variations in the magnitude of latent heat release above the warm frontal region, producing stronger upper-tropospheric downstream ridging in simulations with less PBL mixing. The more amplified flow pattern impedes the northeastward propagation of the surface cyclone and results in a westward shift of precipitation. In addition, trajectory analysis indicates that ascending parcels in the less-mixing simulations condense more water vapor and terminate at a higher potential temperature level than do ascending parcels in the more-mixing simulations, suggesting stronger latent heat release when PBL mixing is reduced. These results suggest that spread within ensemble forecast systems may be improved by perturbing PBL mixing parameters that are not well constrained.

**KEYWORDS:** Boundary layer; Extratropical cyclones; Model comparison; Numerical weather prediction/forecasting; Parameterization

## 1. Introduction

The accurate representation of turbulent mixing processes within the planetary boundary layer (PBL) is an important component of numerical weather prediction over a variety of spatial and temporal scales. Several studies have investigated the sensitivity of atmospheric phenomena, including severe weather outbreaks, tropical cyclones (TCs), and baroclinic waves, to PBL and surface layer parameterization schemes and configurations (Adamson et al. 2006; Beare 2007; Plant and Belcher 2007; Kepert 2012; Boutle et al. 2014; Cohen et al. 2015, 2017; Bu et al. 2017). The demonstrated sensitivity to PBL and surface layer processes inspires the current work of identifying pathways through which subgrid-scale mixing projects on larger-scale features within full-physics simulations. We seek to understand how and to what degree varying boundary layer mixing strength impacts the development and evolution of an extratropical cyclone using Weather Research and Forecasting (WRF) Model simulations of the 26–29 January 2015 eastern U.S. snowstorm.

It has been well established that boundary and surface layer processes play an important role in baroclinic cyclone evolution (Valdes and Hoskins 1988; Adamson et al. 2006; Beare 2007; Plant and Belcher 2007; Boutle et al. 2014). Valdes and Hoskins (1988) investigated the baroclinic instability of a zonal-mean flow and found surface friction can reduce growth rates of baroclinic systems by 50%. Adamson et al. (2006) described how surface friction can influence and dampen

baroclinic systems through Ekman pumping and baroclinic potential vorticity (PV) generation. Plant and Belcher (2007) built on the results of Adamson et al. (2006), analyzing the impacts of surface momentum and heat fluxes on the evolution of baroclinic cyclones. The basic features of the PBL-driven damping mechanisms were found to be robust for different frontal structures, surface heat fluxes, and for a range of surface roughness. Beare (2007) and Boutle et al. (2014) performed a series of experiments selectively switching off boundary layer mixing over stable and unstable surface layers within an idealized cyclone. This was achieved by determining, at each time step, whether the sign of the surface buoyancy flux was negative (stable) or positive (unstable). Their results suggested Ekman pumping and baroclinic PV generation were mostly associated with unstable and stable boundary layers, respectively, and both mechanisms contributed about equally to the dampening of the baroclinic wave.

The impacts of PBL momentum and heat fluxes have been the focus of several baroclinic cyclone studies but the influence of PBL moisture fluxes on baroclinic cyclones has received less attention. Considering the role of condensational heating in extratropical cyclogenesis has been well documented (e.g., Reed et al. 1988; Davis and Emanuel 1988; Kuo et al. 1990; Davis 1992; Davis et al. 1993; Whitaker and Davis 1994; Stoelinga 1996; Brennan and Lackmann 2005), it stands to reason moisture fluxes from the PBL may have a considerable impact on cyclone evolution. Hong and Pan (1996) and Hong et al. (2006) demonstrated changes in PBL mixing strength can impact CAPE and equivalent potential temperature; where shallower, less-intense PBL mixing traps moisture in the lower levels, increasing CAPE and low-level equivalent potential

*Corresponding author:* Matthew T. Vaughan, mvaughan@albany.edu

DOI: 10.1175/MWR-D-20-0264.1

© 2021 American Meteorological Society. For information regarding reuse of this content and general copyright information, consult the [AMS Copyright Policy](#) ([www.ametsoc.org/PUBSReuseLicenses](http://www.ametsoc.org/PUBSReuseLicenses)).

temperature. It is plausible that changes in the mixing of moisture via the PBL may impact the evolution of baroclinic cyclones through augmenting CAPE and low-level equivalent potential temperature fields as latent heat release, particularly around the warm conveyor belt (Carlson 1980; Wernli and Davies 1997; Schemm and Wernli 2014) can substantially impact extratropical cyclogenesis (Reed et al. 1988; Kuo et al. 1990; Stoelinga 1996; Ahmadi-Givi et al. 2004; Joos and Wernli 2012; Binder et al. 2016).

Inspired by the prior literature, one can surmise baroclinic cyclone evolution may be sensitive to the selection of the PBL parameterization scheme. While several studies have addressed the impact of parameterized PBL mixing on baroclinic cyclones, the authors have found no previous literature investigating how variations in PBL mixing strength project on to the baroclinic-cyclone-scale flow, particularly within moist simulations. Boutle et al. (2009) suggests implementing a PBL scheme within an idealized simulation of a moist baroclinic cyclone reduces eddy kinetic energy and leads to a weaker surface pressure minimum (Boutle et al. 2009; their Fig. 2) than a simulation without a PBL scheme, but no further investigation is provided by the authors because a thorough comparison between these two simulations was not the focus of their paper. Our motivations to address how variations in PBL mixing strength project to the larger, cyclone-scale flow are twofold. First, there is an important concern whether baroclinic cyclone evolution is sensitive to reasonable changes in PBL mixing strength. Second, the impact of PBL mixing strength on the distribution of moisture is an important consideration for determining convective activity in the outer core of TCs (Bu et al. 2017). Therefore, it is hypothesized that latent heating differences arising from variations in low-level moisture distributions, coincident with changes in PBL mixing, can impact the evolution of baroclinic cyclones through diabatic ridge building (Stoelinga 1996). Under these circumstances, this work may help to improve forecast skill through revealing sources of variability in simulated cyclogenesis arising from uncertainty in PBL mixing parameters.

In this paper, we investigate how variations in parameterized PBL mixing can impact the evolution of a moist baroclinic cyclone as described in section 2. WRF PBL parameterization schemes and simulation parameters are also discussed in section 2. Section 3 presents results from various sensitivity experiments in an Eulerian framework and suggests a primary mechanism by which variations in PBL mixing strength impact a baroclinic cyclone. The various experiments are summarized in Table 1, and each simulation is further explained within the text below. Trajectory analyses are presented in section 4 to further expand upon the findings in section 3, and a discussion and summary are presented in section 5.

## 2. Background and methods

### a. PBL schemes in the Weather Research and Forecasting Model

PBL parameterizations seek to replicate the effects of subgrid-scale turbulent mixing of heat, momentum, and moisture by

TABLE 1. Summary of experiments.

Expt name	Description
ACM2	ACM2 PBL scheme
MYNN	MYNN PBL scheme
Less mixing	Default YSU PBL scheme (CRN = 0.00)
More mixing	YSU PBL scheme with CRN = 0.25
Less-mixing SKEBS	Five-member less-mixing ensemble with SKEBS perturbations
More-mixing SKEBS	Five-member more-mixing ensemble with SKEBS perturbations
NOLH less mixing	Same as less mixing but without latent heating
NOLH more mixing	Same as more mixing but without latent heating
MOISTMIX	Same as less mixing but with CRN = 0.25 for moisture mixing

calculating vertical diffusion coefficients that are applied to predictive equations for momentum and scalars, such as temperature and moisture, during model runtime. At this writing, the vast majority of PBL schemes are one-dimensional, acting on model columns individually and independently of neighboring columns. There are several PBL mixing parameterization strategies used in numerical weather prediction models and many schemes rely on the concept of eddy diffusivity to find the turbulent vertical flux of a quantity (e.g., heat, momentum, and moisture). Adapting Eq. (3.1) from Holtslag and Boville (1993), vertical turbulent flux can be written as

$$\overline{w'C'} = K_c \frac{\partial C}{\partial z} + N_{NL}, \quad (1)$$

where  $C \in (q, \theta, u, v)$ ,  $K_c$  is the eddy diffusivity for  $C$ , and  $N_{NL}$  represents nonlocal terms that vary among schemes.

PBL parameterizations can be binned in one of two groups depending on the strategy used to close the turbulence equations and obtain  $K_c$ : turbulent kinetic energy (TKE) schemes and bulk  $K$ -profile schemes. TKE-based PBL parameterizations, such as the Mellor–Yamada–Nakanishi–Niino (MYNN) scheme (Nakanishi and Niino 2009; Olson et al. 2019), use variables or gradients of variables vertically adjacent to a given point to determine the amount of vertical mixing at that point (Cohen et al. 2015). As a result, TKE schemes develop an eddy diffusivity profile, with contemporary schemes of at least 1.5 order using prognostic equations for TKE to derive eddy diffusivities within a column for heat, momentum, and moisture. The  $K$ -profile schemes, such as the Yonsei University (YSU) scheme (Hong et al. 2006), determine the PBL height and impose an empirical eddy diffusivity profile through the PBL. Some modern schemes, such as the Asymmetric Convective Model, version 2 (ACM2; Pleim 2007), incorporate concepts from both TKE and  $K$ -profile closure approaches, so herein we consider it as a third type of scheme.

Many PBL schemes featuring a  $K$ -profile closure approach, such as ACM2 and YSU, utilize a critical Richardson number (CRN) to determine PBL height and, consequently, control the depth and strength of the imposed eddy diffusivity profile. First, a bulk Richardson number (BRN) is computed

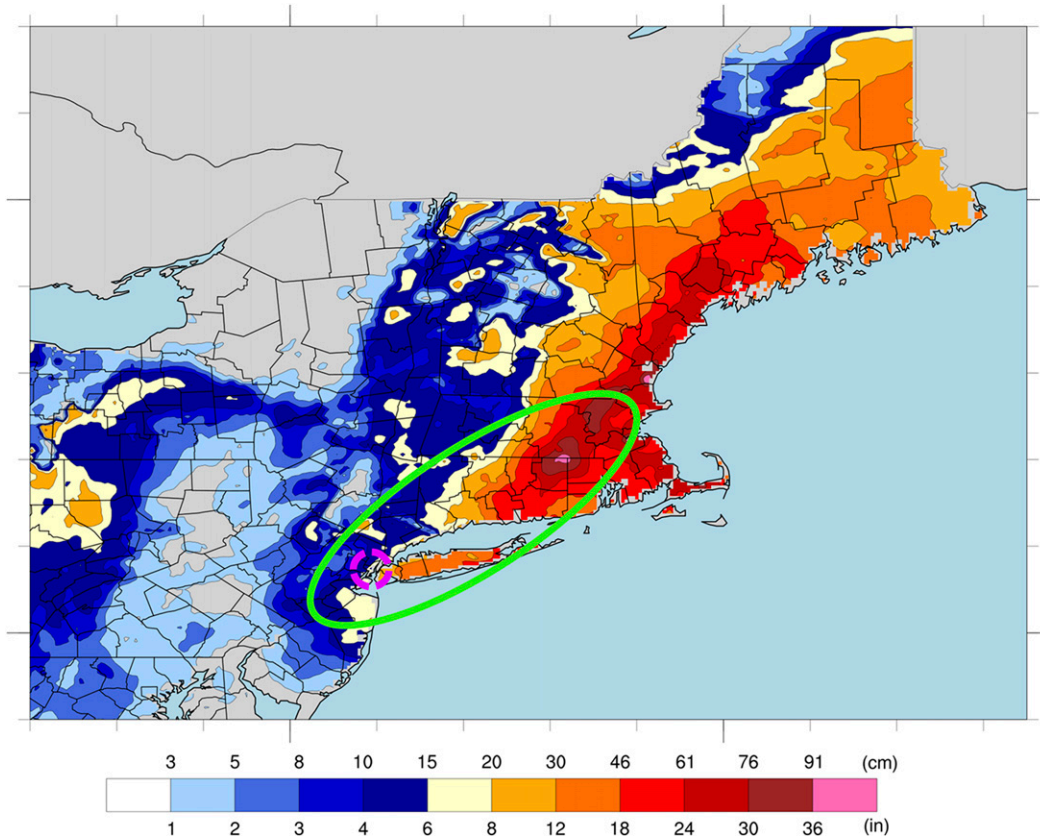


FIG. 1. National Operational Hydrologic Remote Sensing Center 48-h snowfall accumulation (shading; cm, with inch scale also included) ending at 1200 UTC 28 Jan 2015. The green oval outlines the I-95 corridor discussed in the text, and the magenta dashed circle highlights the location of New York City.

for each grid column. Hong (2010) defines the BRN in the YSU as

$$BRN(z) = \frac{g(\theta_v - \theta_s)z}{\theta_{va} U(z)^2}, \quad (2)$$

where  $\theta_v$  is the virtual potential temperature,  $\theta_s$  is the near-surface virtual potential temperature,  $\theta_{va}$  is the virtual potential temperature at the lowest model level, and  $U(z)$  is the wind speed at height  $z$ . The BRN is calculated from the surface to progressively higher levels until the CRN is reached. In YSU, a surface thermal excess term is applied to  $\theta_s$ , in unstable conditions, and the BRN is recalculated to obtain the final PBL height. ACM2 uses a similar approach except the BRN is calculated over the entrainment layer only, starting at the level of neutral buoyancy with respect to rising surface layer air parcels (Pleim 2007) rather than the surface.

Several studies have investigated how changing the CRN in  $K$ -profile schemes impacts model performance (Hong and Pan 1996; Cohen et al. 2017; Bu et al. 2017). Other factors being equal, a smaller CRN lowers the PBL height and reduces eddy diffusivity through the PBL when compared with a larger value (Kepert 2012). In the present study, it is shown in section 3 that varying the CRN in a single  $K$ -profile PBL scheme is useful to achieve variability in PBL mixing strength while simplifying

the experiment by limiting the number of variables and isolating the depth and strength of the imposed eddy diffusivity profile as the source of sensitivity within the simulations.

*b. 26–29 January 2015 snowstorm and model setup*

The 26–29 January snowstorm brought heavy snow to many portions of the northeastern United States, particularly along the Interstate Highway 95 (I-95) corridor (Fig. 1). An upper-level trough propagated southeastward out of Canada and amplified as it approached the U.S. coastline, resulting in the formation of a sub-984-hPa coastal surface cyclone. The intense snowfall in New England and the sharp gradient in snowfall on the western edge of the storm made the event particularly notorious. The tight snowfall gradient contributed to considerable forecast uncertainty with regard to precipitation totals along the coast, especially in New York (City), New York, and surrounding areas of New Jersey.<sup>1</sup> A more detailed review of this event is provided by Greybush et al. (2017) who

<sup>1</sup> The difficult snowfall forecast resulted in an apology issued by an NWS meteorologist at the Mount Holly, New Jersey, forecast office via personal Twitter account (Babay 2015), which, to the authors’ knowledge, is an unusual occurrence.

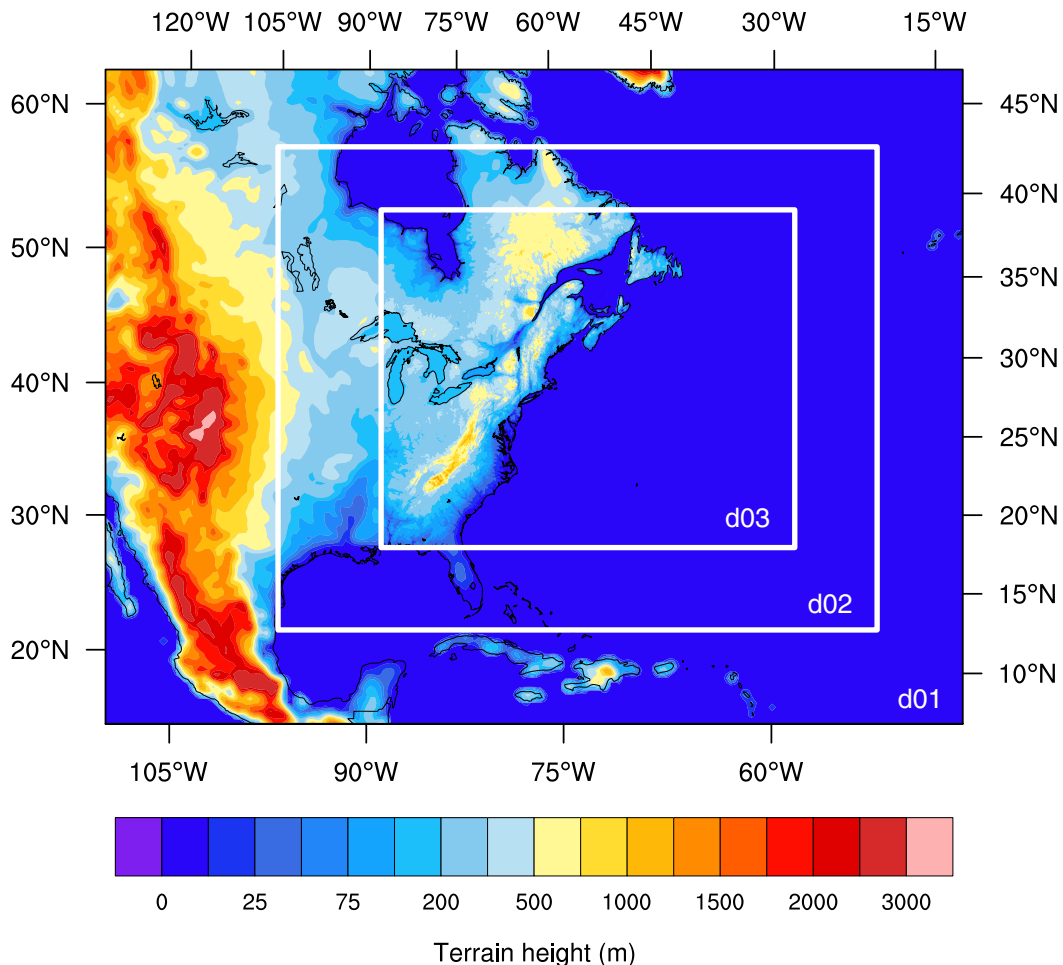


FIG. 2. Telescoping configuration employed for the WRF simulations in this study, consisting of three (36-, 12-, and 4-km horizontal grid spacing) domains. The topography of the outermost domain is shown (shading), except where superimposed with 4-km (Domain 3) terrain.

linked uncertainties in snowfall location to variations in the position of the coastal low.

The WRF Model's Advanced Research WRF core, version 3.7.1, incorporating ERA-Interim (European Centre for Medium-Range Weather Forecasts 2009; Dee et al. 2011) data for initial and boundary conditions, is employed to conduct 72-h simulations of the snowstorm initialized at 0000 UTC 26 January 2015. Three telescoping domains, with horizontal grid spacings of 36, 12, and 4 km (Fig. 2), are employed, and our model physics and vertical resolution are similar to the High-Resolution Rapid Refresh model described in Benjamin et al. (2016) except we use the modified MM5 surface layer scheme (Jiménez et al. 2012), Noah land surface model (Ek et al. 2003), and a variety of PBL schemes. The surface layer scheme is responsible for computing the transfer coefficients for momentum and scalar fluxes from the land surface model to the atmosphere. Consequently, PBL schemes in WRF rely on the surface fluxes computed from the surface layer to estimate subgrid-scale mixing and are often paired with unique surface layer schemes. Recent research has shown

considerable variability surrounding how fluxes and frictional effects are calculated within surface layer schemes available in WRF (Minder et al. 2020). Therefore, to simplify the experiment and focus our study on the effects of PBL parameterizations, we use a single surface layer scheme, the modified MM5, because of its compatibility with several PBL schemes.

Several sensitivity tests are conducted to examine how robust cyclone evolution sensitivity is to various physics configurations. A 10-member ensemble is created using the Stochastic Kinetic Energy Backscatter technique (SKEBS; Berner et al. 2011) to test whether differences in cyclone evolution, arising from variations in PBL mixing, are consistent. The SKEBS scheme assumes that upscale and downscale cascading energy results in forcing for the resolved flow from unresolved scales with a perturbation amplitude proportional to the instantaneous dissipation rate. The SKEBS scheme, outlined in Berner et al. (2011) and implemented in WRF, includes a constant dissipation rate in space and time, allowing the perturbations to be considered as additive noise to the horizontal velocity ( $u$  and  $v$ ) components and potential



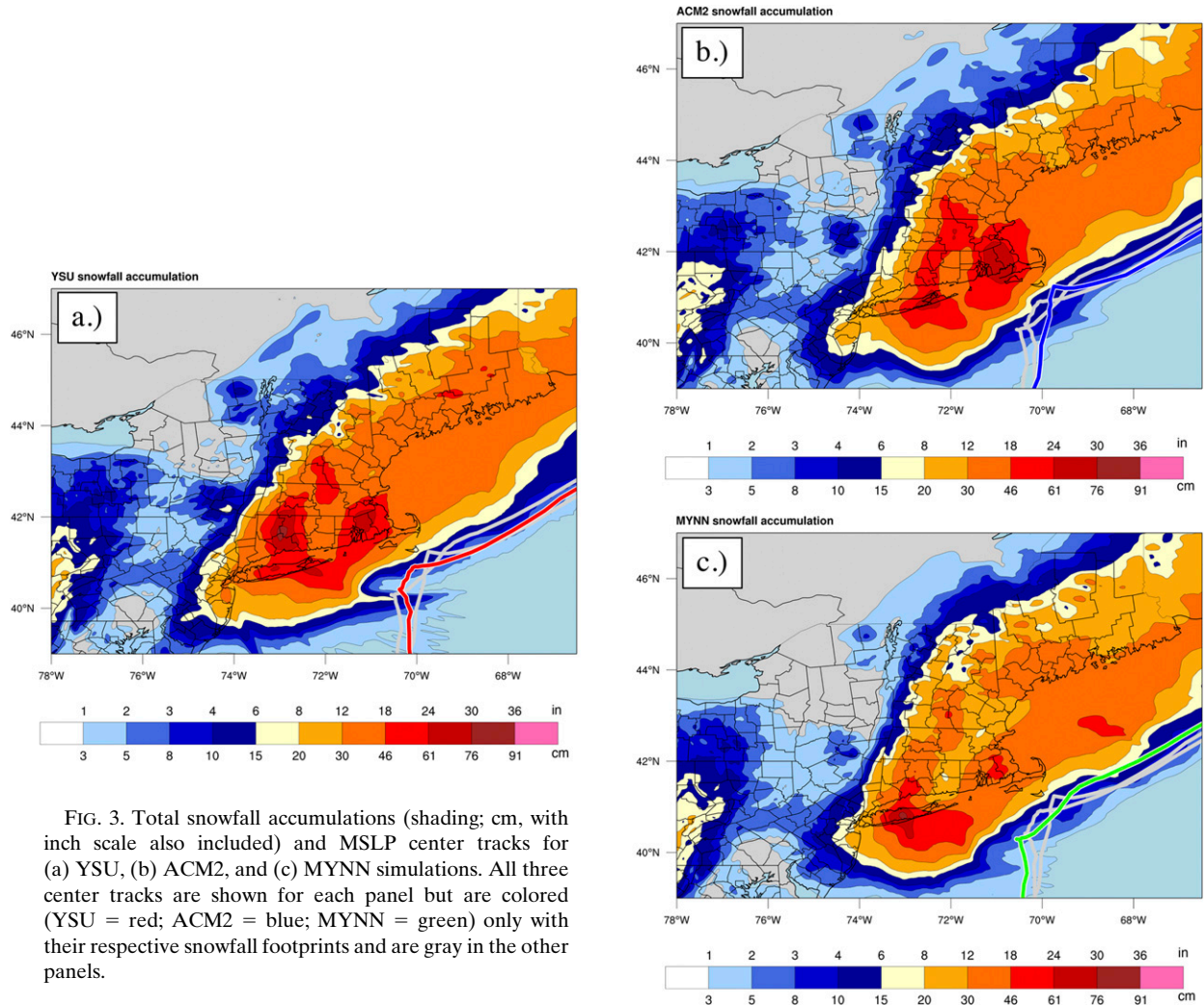


FIG. 3. Total snowfall accumulations (shading; cm, with inch scale also included) and MSLP center tracks for (a) YSU, (b) ACM2, and (c) MYNN simulations. All three center tracks are shown for each panel but are colored (YSU = red; ACM2 = blue; MYNN = green) only with their respective snowfall footprints and are gray in the other panels.

temperature  $\theta$  fields with prescribed spatial and temporal correlation (Duda et al. 2016). SKEBS parameters used for the ensemble, such as the magnitude and scale of the perturbations, follow the recommended values (National Center for Atmospheric Research 2015, 5–26).

In light of prior work with regard to sensitivity to surface friction and heat fluxes, it stands to reason that the variety of methods used to determine PBL mixing may result in differences in cyclone evolution. Simulations of the 26–29 January snowstorm are performed using the MYNN, YSU, and ACM2, representing the three categories of PBL schemes described above. Results, presented in section 3, indicate considerable diversity among the simulations warranting further study of how baroclinic cyclones are affected by the representation of PBL mixing within a numerical weather prediction model.

Trajectories, shown in the section 4, are computed using LAGRANTO (Sprenger and Wernli 2015) utilizing hourly model output. All model fields shown are using the innermost 4-km domain unless specified otherwise. All snowfall accumulations presented herein use a 10:1 snow-to-liquid for

consistency. A 10:1 ratio was chosen to approximate the climatological snow-to-liquid ratio for the coastal northeastern United States in March (Baxter et al. 2005; their Fig. 8); however, we are most interested in the spatial pattern of snowfall for this study rather than the snowfall amounts.

### 3. Sensitivity experiments and results

#### a. Proof of concept and control runs

As a proof-of-concept experiment, three 72-h simulations of the 26–29 January 2015 snowstorm are performed using the MYNN, YSU, and ACM2 PBL schemes, to establish whether any facet of baroclinic cyclone evolution is sensitive to the selection of PBL parameterization scheme. The mean sea level pressure (MSLP) centers in all simulations vary somewhat as the systems organize, but the cyclones generally follow a northward track before turning northeastward off the New England coastline (Fig. 3). While MSLP tracks overlap somewhat, there are subtle yet important differences, particularly in

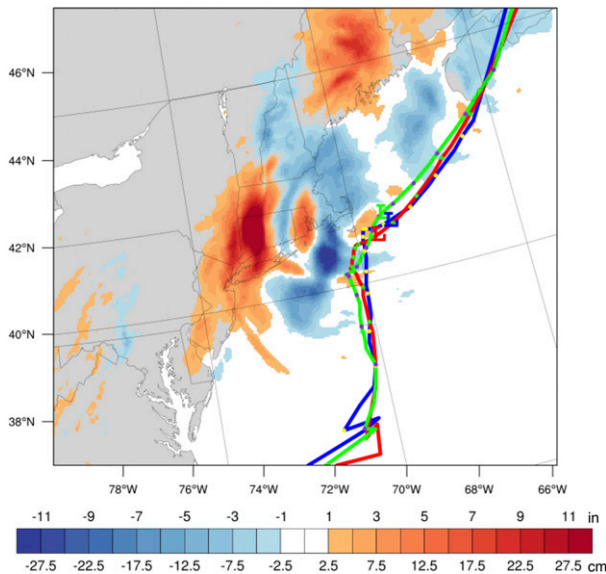


FIG. 4. MSLP center tracks for YSU (red), ACM2 (blue), and MYNN (green) simulations. For each color-coded simulation, dots are 3-hourly surface cyclone center locations and L represents the surface low center location at 0600 UTC 28 Jan 2015. Also shown is total snowfall accumulation (YSU – ACM2; cm, with inch scale also included; shading).

the propagation of the surface cyclone centers. Concomitant with the variations in track are marked differences in snowfall footprints among the three simulations. This may be anticipated because of the demonstrated relationship between the 26–29 January surface cyclone track and snowfall location and intensity by Greybush et al. (2017) (their Fig. 2). The MYNN, which uses a TKE approach to diagnose subgrid-scale mixing, generates an area of heavy snowfall greater than 61 cm on Long Island (Fig. 3c), similar to the YSU (Fig. 3a) and ACM2 (Fig. 3b) runs, but produces less snowfall across the domain elsewhere. The ACM2 and YSU snowfall footprints are more similar but the YSU snowfall footprint is shifted to the west (Figs. 4a,b), which can be (and in this case, is) important because the storm tracks run very close to large metropolitan areas. Discrepancies in forecast precipitation around densely populated regions, such as those seen here between the YSU and ACM2 simulations, can lead to substantial variations in forecast societal impacts.

While the hybrid ACM2 scheme and  $K$ -profile YSU scheme differ in many ways, both use a CRN to diagnose the PBL height and impose a  $K$  profile [ $K_c$  in Eq. (1)] that establishes the amount of mixing between adjacent vertical grid levels within the PBL. The ACM2 scheme uses a default CRN of 0.25 for unstable surface layers while the YSU scheme uses a CRN of 0.00 for the same (Pleim 2007; Hong 2010). A CRN of 0.25 allows diagnosis of the PBL top to be within the capping inversion of a classic convective boundary layer, permitting implicit mixing and entrainment at the top of the boundary layer. A CRN of 0.00 limits implicit entrainment; therefore, YSU calculates PBL-top entrainment explicitly using an additional term under  $N_{NL}$  of Eq. (1).

An important difference between the two parameterizations, aside from their default CRNs and the layers over which they calculate the BRN, is how each scheme computes upward and downward mixing. ACM2 is a hybrid, or “asymmetric,” scheme, meaning that upward and downward mixing rates are defined separately: upward mixing is dependent on both local gradients of mixed variables (e.g., heat, momentum, and moisture) and an imposed mixing profile dependent on surface buoyancy and the CRN, whereas downward mixing is related to upward mixing through mass conservation but only uses local gradients to derive downward mixing rates (Pleim 2007). YSU also imposes an eddy diffusivity profile derived from surface fluxes and the CRN, but treats upward and downward mixing equally. While these unique characteristics likely contribute to the variations in storm-total snowfall seen in Fig. 4, we wish to explore whether the differences between these schemes may be approximated by modifying the CRN.

### b. Proxy runs

In an attempt to resolve the processes by which these PBL schemes impact a baroclinic cyclone, we seek to reduce the degrees of freedom of the experiment by using a single PBL scheme with modified mixing parameters to capture the variability seen in Fig. 4. Therefore, we conduct another simulation using the YSU scheme, but now with a CRN of 0.25 like ACM2. This simulation will be referred to as “more mixing” and the original YSU run with CRN of 0.00 will be termed “less mixing.” We then investigate whether changing a single mixing parameter yields similar variability seen between the original YSU and ACM2 simulations (Fig. 4). Note that raising the CRN to 0.25 permits both implicit and explicit PBL mixing within the YSU due to the PBL-top entrainment term mentioned above. We performed CRN = 0.25 experiments with and without the parameterized entrainment and noted little impact on surface cyclone movement and similar snowfall footprints (not shown). As a consequence, for simplicity, the more-mixing experiments described herein have retained the PBL-top entrainment.

Initially, the MSLP fields of the less-mixing and more-mixing simulations evolve similarly, but the locations of the surface low centers begin to diverge around forecast hour 40 (i.e., 1600 UTC 27 January) as the cyclones approach the time of minimum MSLP (Fig. 5a). The surface low pressure center in the more-mixing case begins to move northeastward relative to the surface low pressure center in the less-mixing case (Figs. 5b,c), which appears to stall off the New England coast (Fig. 5c inset), leading to a difference in cyclone center locations on the order of 80 km by 0600 UTC 28 January. This relative orientation persists until approximately 1500 UTC 28 January as the surface cyclones occlude and their respective central pressure minima become less defined. The differences in stalling behavior and cyclone propagation between the two YSU runs, although ostensibly small, contribute to a considerable change in snowfall location and intensity (Fig. 5d) that is impactful, again owing to the storms’ proximity to densely populated areas. Note the less-mixing simulation produces more snowfall on the western flank of the cyclone over western New England and eastern New York.

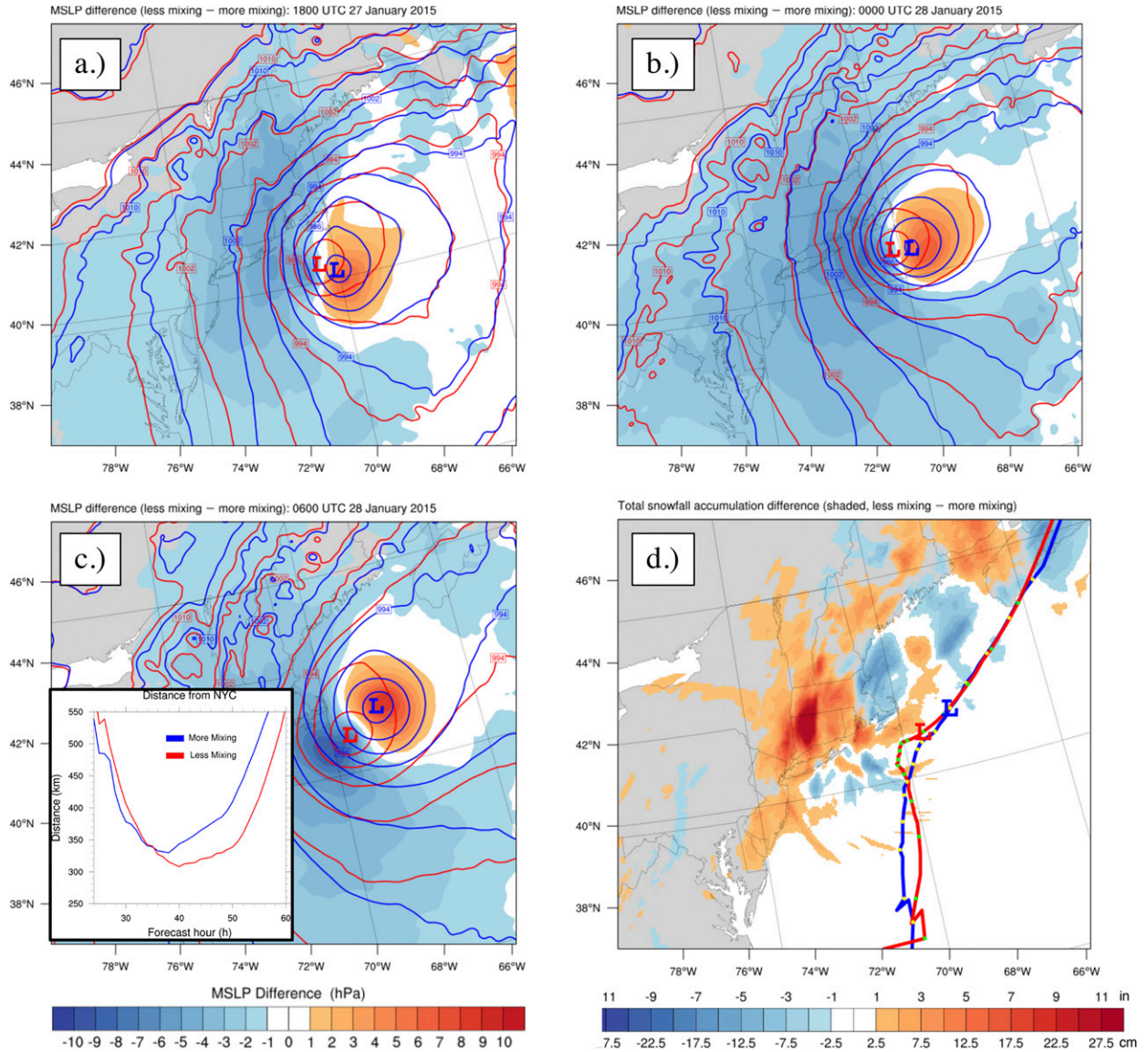


FIG. 5. MSLP (hPa; contours) for less-mixing run (red) and more-mixing run (blue) and MSLP difference (less mixing – more mixing; hPa; shading) valid at (a) 1800 UTC 27 Jan, (b) 0000 UTC 28 Jan, and (c) 0600 UTC 28 Jan. (d) As in Fig. 4, but for the less-mixing (red) and more-mixing (blue) simulations. The inset in (c) is the surface cyclone distance (km) from New York City for less-mixing (red) and more-mixing (blue) runs.

Despite the similarities between the more-mixing and ACM2 runs (Fig. 6), the more-mixing simulation does not replicate some other aspects of the ACM2 case, suggesting there are factors other than the CRN that control PBL mixing and how that mixing projects to larger scales. Nevertheless, the more rapid movement of the more-mixing run’s cyclone demonstrates that the CRN may be manipulated to provide a reasonable spread in model solutions resembling what can be expected using different PBL physics.

The larger CRN of the more-mixing simulation induces stronger eddy diffusivity within the PBL than the less-mixing simulation, which is a direct consequence of it encouraging relatively deeper boundary layers. This can be seen in an

area-average profile taken through the warm sector of the cyclone (Fig. 7a). Here, the warm sector is delineated by first computing the average and standard deviation of the 950–800-hPa potential temperature across the innermost domain at a given time and using this to convert the field into standardized anomalies. Next, to create the profiles, we average only those grid points possessing a positive value (i.e., the “warm” values; Fig. 8). This technique divides the domain into two equal parts at each time for each simulation and seeks to prevent cold sector profiles, which are predominately unstable in an oceanic cyclone owing to strong cold-air advection over warmer waters, from obscuring differences in the warm-sector PBLs.



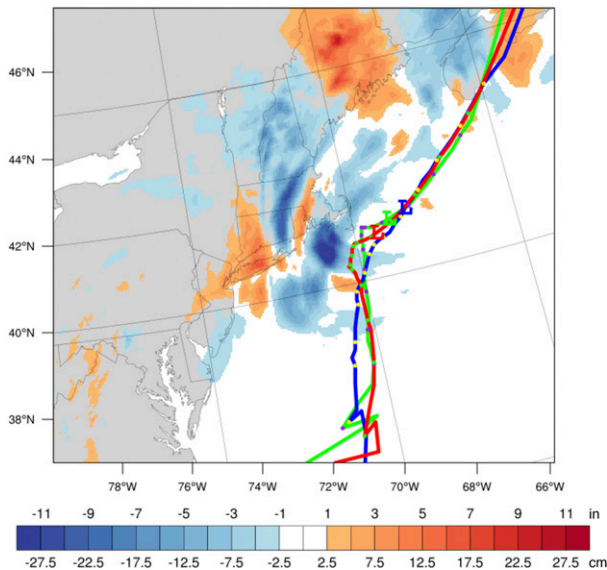


FIG. 6. As in Fig. 4, but for more mixing (blue) – ACM2 (green), with less mixing (red) shown for reference.

As anticipated, area-averaged vertical profiles of eddy diffusivity for scalars<sup>2</sup> indicate stronger mixing over a deeper depth in the more-mixing simulation (Fig. 7a). The differences in eddy diffusivity result, predictably, in higher wind speeds at the surface and lower wind speeds aloft in the more-mixing simulation (Fig. 7b). Furthermore, the vertical moisture profile suggests the lowest levels (below 800 m) of the PBL are more moist in the less-mixing case and drier aloft (Fig. 7c). Reduced mixing limits both entrainment of free tropospheric air into the PBL and inhibits the upward mixing of moisture away from the near-surface where moisture content is largest, thereby preserving moisture in the sub-800-m layer.

In an attempt to link the enhanced PBL mixing with reduced near-surface moisture, accumulated boundary layer mixing ratio (ACBLQ) is computed during the model integrations. ACBLQ is calculated by multiplying the instantaneous tendency in vapor mixing ratio from the PBL scheme by the time step (24 s for the innermost domain) and binning the result for each grid volume. Consequently, ACBLQ describes the degree to which the PBL scheme is moistening (positive values) or drying a grid volume since model initiation. Figure 7d indicates the PBL scheme in the less-mixing simulation is moistening the lowest 800-m layer of the warm sector more than the more-mixing run. This suggests the instantaneous moisture differences at 1800 UTC 27 January are associated with PBL moisture tendency variations derived from changes in PBL mixing strength.

<sup>2</sup> The eddy diffusivity of scalars is related to the eddy diffusivity of momentum through the Prandtl number that, while allowed to vary with height in the YSU, produces a momentum diffusivity profile shape (not shown) that is similar to that seen in Fig. 7a.

### c. SKEBS experiment

Motivated by the above experiment, a SKEBS ensemble based on the proxy runs is created to test the robustness of the demonstrated variations in surface cyclone movement. Again, the SKEBS scheme adds stochastic, small-amplitude perturbations to the rotational component of the horizontal wind and potential temperature tendency equations at each time step (Berner et al. 2011). This additive noise approach essentially creates different versions of the January snowstorm to assess the consistency of the relationship between cyclone track and mixing strength. The ensemble consists of 10 members using the same domains in Fig. 2, 5 being less-mixing (i.e., default YSU) members along with 5 more-mixing YSU members using a CRN of 0.25.

Each ensemble member from the less-mixing group is paired with its more-mixing counterpart employing the same random seed. The results suggest the SKEBS perturbations add more spread to the model solution than changing the CRN alone (Figs. 9a–c). This may be anticipated given the SKEBS perturbations are added through the entire depth of the model atmosphere.<sup>3</sup> However, the MSLP and precipitation difference patterns, highlighted in the previous experiment, are persistent among the ensemble sets (Figs. 9a–c). The ensemble mean differences of MSLP low location and accumulated snowfall between the two mixing regimes (Fig. 9d) is consistent with the difference patterns illustrated by the individual ensemble sets. The surface cyclones in the more-mixing ensemble move more rapidly toward the north and east relative to their less-mixing counterparts in each of the five pairs and the ensemble mean (three sets and the ensemble mean shown for clarity in Figs. 9a–d). These results suggest the tendency of the more-mixing surface cyclone to move more quickly north and east is unlikely to be explained by random chance.

### d. Latent heat and moisture sensitivity runs

It was hypothesized in section 1 that moisture content within the PBL could affect the evolution of a baroclinic cyclone through modifying latent heat release. An experiment is conducted where latent heating is turned off (NOLH) within the model starting at 0000 UTC 27 January (forecast hour 24) to assess the importance of latent heat release to the evolution of each cyclone.<sup>4</sup> The surface cyclones in the NOLH experiment progress along the east coast of the United States, in general agreement with the less-mixing/more-mixing experiment, but fail to deepen to the same degree as in the full-physics simulations. Additionally, the less-mixing surface cyclone moves *faster* to the north and east than its more-mixing counterpart (Fig. 10), contrary to the simulations with latent heating

<sup>3</sup> Although PBL schemes apply vertical mixing through the entire model column, it stands to reason that the largest differences are confined below the boundary layer height where eddy mixing is usually most vigorous.

<sup>4</sup> We remove latent heating after 24 h into the simulation because of the lack of an organized surface cyclone in runs with no latent heating beginning at initialization, making them unsuitable for comparison here.



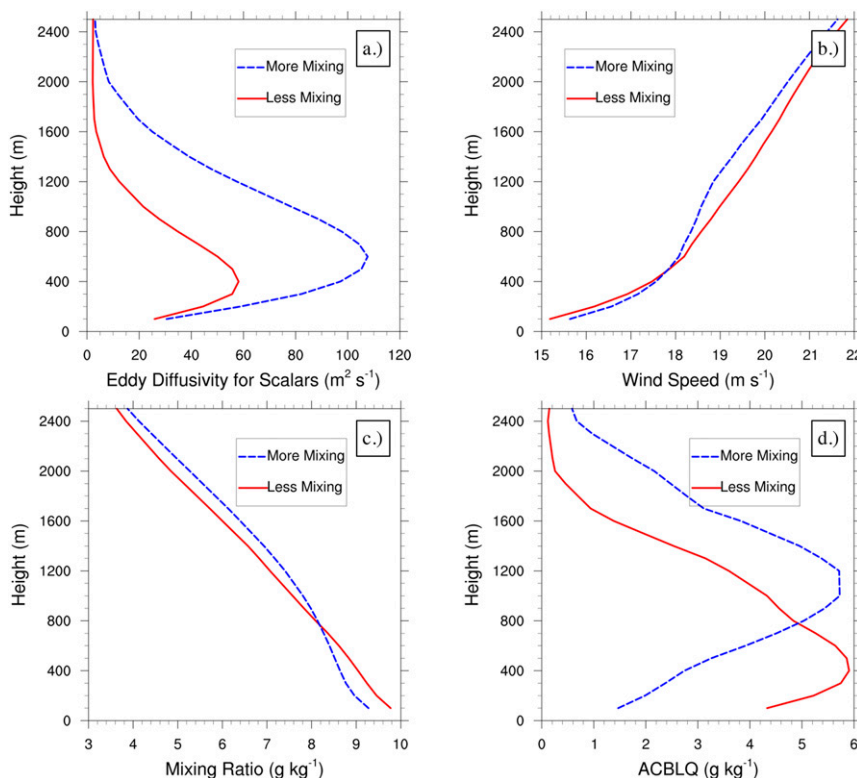


FIG. 7. Warm-sector area-averaged vertical profiles for less-mixing (red) and more-mixing (blue) simulations of (a) eddy diffusivity, (b) wind speed, (c) mixing ratio, and (d) accumulated boundary layer mixing ratio valid at 1800 UTC 27 Jan. Area averaging is accomplished by calculating the 950–800-hPa potential temperature anomaly for 1800 UTC 27 Jan across the innermost domain (Fig. 8, below) and averaging over the area of positive potential temperature anomalies for each simulation.

(Fig. 5d). This difference in cyclone progression is consistent with the inverted snowfall difference pattern relative to the full-physics experiment (Figs. 5d and 10). The NOLH more-mixing simulation produces more snow around and to the east of the Hudson Valley region, although snowfall difference magnitudes are smaller than the full-physics proxy runs because of, in part, the weaker NOLH systems.

The results of the NOLH experiment suggest latent heating—and consequently, moisture—play a critical role in how variations in PBL mixing impact baroclinic cyclones. However, removing latent heating drastically alters the evolution and strength of the simulated cyclone to the point where the simulation is no longer representative of the 26–29 January snowstorm. This could be anticipated from Stoelinga (1996), who demonstrated latent heating can have a substantial effect on the low-level circulation field of oceanic cyclones and the subsequent life cycle of the baroclinic system. Thus, a more surgical approach is needed to preserve the general structure and intensity of the snowstorm while assessing the system’s sensitivity to moisture.

To this end, we conduct a YSU experiment (hereafter, MOISTMIX) that increases the CRN used for calculating the eddy diffusivities applied to water species (i.e., vapor and cloud water) to 0.25 while retaining the scheme’s default 0.00 CRN in

the determination of eddy diffusivity of momentum and temperature, again whenever and wherever the surface layer is unstable. This is accomplished by solving for heat, moisture, and momentum tendencies using a modified CRN of 0.25 in the YSU. The unstable regime CRN is then adjusted back to 0.00 and the YSU is allowed to recalculate the temperature and momentum tendencies. In other words, MOISTMIX is the less-mixing run except with respect to water vapor and cloud water mixing, for which it mimics the more-mixing simulation. Results from the MOISTMIX experiment (Fig. 11a) indicate that an increase in eddy diffusivity applied to water species has a similar influence on cyclone propagation and snowfall footprint as increased eddy diffusivity across all scalars and momentum (Fig. 5d), with more precipitation on the western flank of the less-moisture-mixing cyclone relative to the faster-propagating MOISTMIX cyclone. Additionally, MOISTMIX closely matches ACM2 in cyclone track, propagation speed, and snowfall footprint (Fig. 11b), further highlighting the importance of moisture mixing by PBL schemes on cyclone evolution.

The sensitivity of cyclone propagation to the vertical mixing of moisture in the MOISTMIX experiment suggests that latent heating plays a considerable role in differentiating between the two mixing regime simulations demonstrated earlier (Fig. 5d).

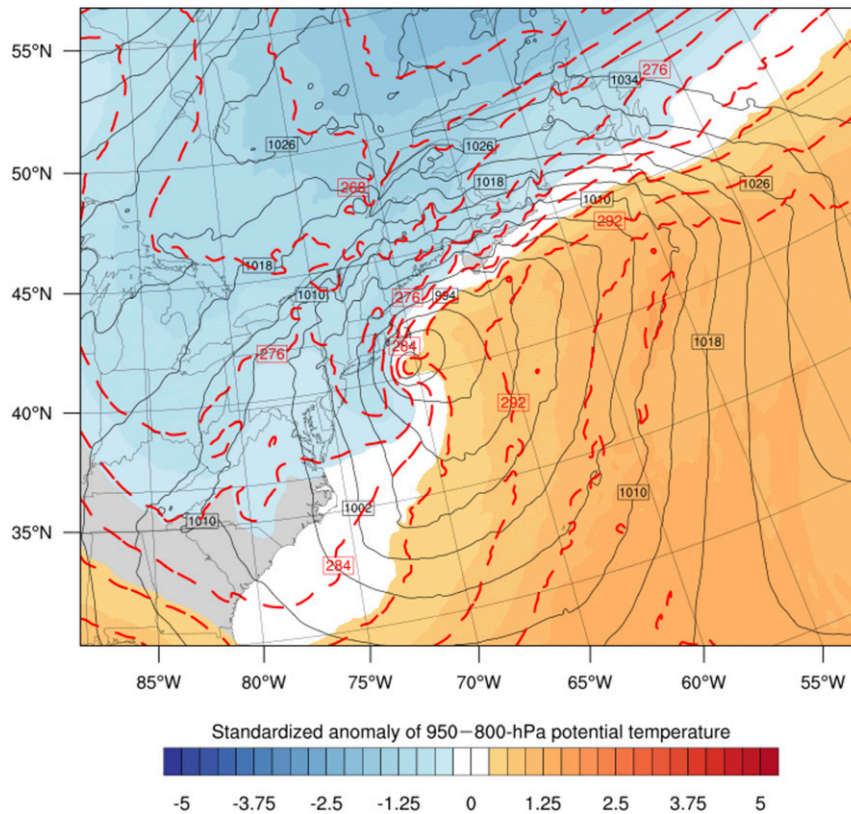


FIG. 8. MSLP (black solid contours; hPa), 950–800-hPa potential temperature (red dashed contours; K), and 950–800-hPa potential temperature standardized anomaly (shading;  $\sigma$ ) for the less-mixing simulation valid at 1800 UTC 27 Jan 2015.

As the less-mixing/more-mixing surface cyclones diverge (Figs. 5a–c), higher upper-level heights aloft develop to the north and east of the less-mixing cyclone (Fig. 12a) compared to its more-mixing counterpart. The higher heights are coincident with warmer temperatures in the 400–300-hPa layer (Fig. 12b) and are consistent with stronger upper-level ridging in the less-mixing simulation (Fig. 12a). It is hypothesized that stronger latent heating in the less-mixing cyclone contributes to stronger ridge building downstream of the surface cyclone through the diabatic term of the quasigeostrophic height tendency equation, which supports forcing for height rises above maximums in diabatic heating. Although not shown, enhanced ridging is present using middle-tropospheric pressure layers (e.g., 400–600 hPa) to the south-southeast of the green outlined area in Fig. 12a suggesting latent heating differences extend along the warm conveyor belt. The 900–500-hPa thickness lines of the less-mixing run are shifted westward of the more-mixing run (Fig. 12c), indicating warmer air extends farther west in the less-mixing run consistent with stronger latent heating in the lower troposphere along the warm conveyor belt.

Recall from Figs. 5a and 5c (inset) that the surface cyclones in both simulations have begun to separate concurrent with the differences in 900–500-hPa thickness shown in Fig. 12c. The primary consequence of the shift in the thickness field is a reduction in thermal wind strength over the less-mixing surface

cyclone, as the strongest gradient in thickness is shifted to the west of the cyclone center (Fig. 12c). Weaker shear above the surface pressure minimum supports the slower propagation speed of the less-mixing cyclone, seen in Figs. 5a–c, according to the thermal steering term of Sutcliffe (1947). The Trenberth form of the quasigeostrophic omega equation (Trenberth 1978) may also be used to explain the variation in cyclone propagation. A weaker thermal wind field around the less-mixing surface cyclone results in weaker advection of middle-troposphere relative vorticity by the thermal wind (not shown) downshear of the surface cyclone, thus reducing both the forcing for upward vertical motion and propagation of the surface cyclone. Furthermore, enhanced ridging and associated upper-level divergence amplify the upper-level flow pattern, producing a deeper trough and a stronger downstream ridge in the less-mixing case (Fig. 12a). These processes, combined with a shortening of the wavelength of the upper-level baroclinic wave due to the aforementioned amplification, likely act to slow the northeastward progression of the surface cyclone.

It is hypothesized that the height differences seen in Fig. 12a are a result of stronger latent heating to the north and east of the surface cyclone in the less-mixing case due to higher PBL moisture content. A CRN of 0.25 results in stronger mixing through a deeper column, reducing water vapor content in the low levels of the PBL while increasing the water vapor content

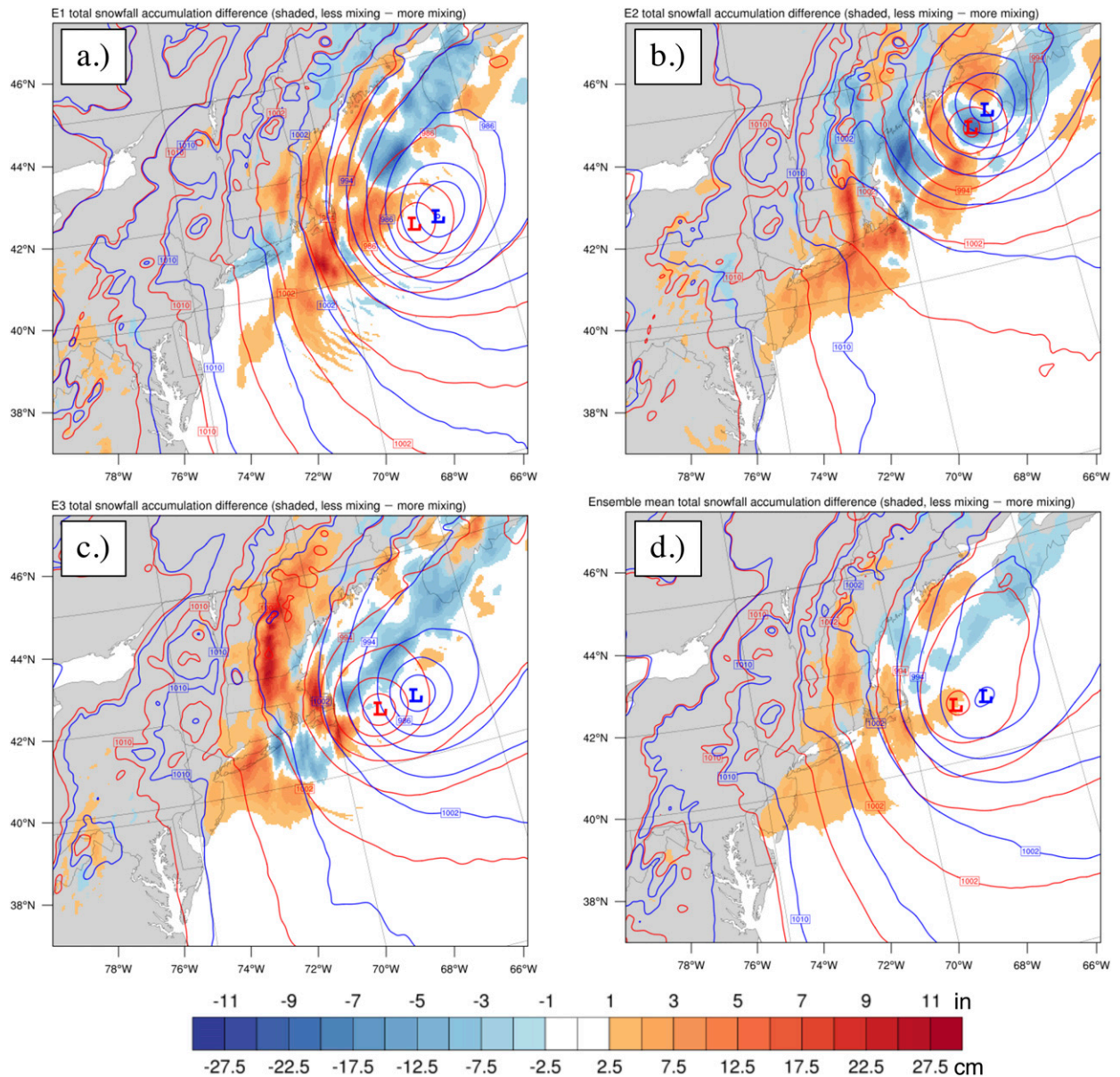


FIG. 9. MSLP (contours; hPa), valid at 0600 UTC 28 Jan, for less-mixing (red) and more-mixing (blue) ensemble trials and total snowfall accumulation difference (less mixing – more mixing; cm, with inch scale also included; shading) for SKEBS trials (a) 1, (b) 2, (c) 3 and (d) the ensemble mean.

aloft (Figs. 7c,d). The higher moisture values below 800 m in the less-mixing case (Fig. 7c) suggest weaker PBL mixing effectively preserves PBL moisture, leading to the higher warm-sector MUCAPE values seen at all times through the simulations (Fig. 13). This is consistent with the findings of Hong et al. (2006), who found weaker mixing resulted in higher CAPE and higher moisture values trapped near the surface. Higher water vapor content and larger MUCAPE may lead to stronger condensational heating through ascent above the warm front as parcels originating in the PBL are lifted via the warm conveyor belt. The dynamic nature of the warm conveyor belt motivates a Lagrangian approach to analyze how differences in low-level

moisture content may impact upper-level flow patterns and, subsequently, surface cyclone propagation, in the next section.

#### 4. Trajectory analysis

Trajectory analysis, using the LAGRANTO (Sprenger and Wernli 2015) software package adapted for WRF, is conducted to investigate the origins of the height differences between the less-mixing/more-mixing simulations (Fig. 12a). LAGRANTO was selected for this work due to its computational efficiency, ease of use for calculating trajectory swarms, and compatibility with WRF. Swarms of 24-h backward trajectories are launched



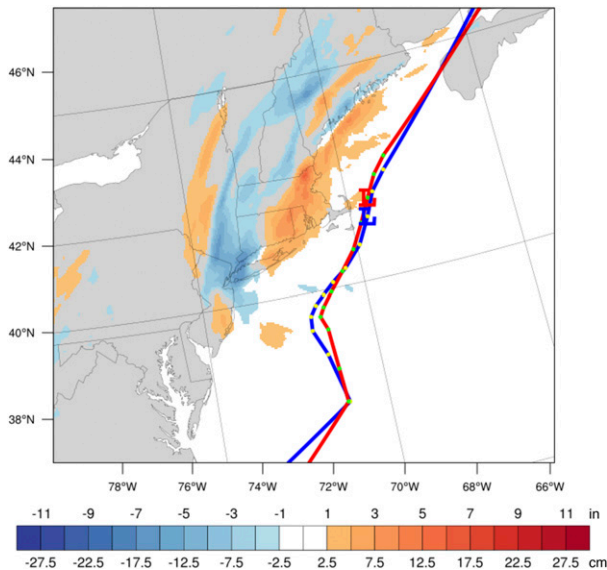


FIG. 10. As in Fig. 4, but for the less-mixing (red) and more-mixing (blue) simulations without latent heating.

within the less-mixing/more-mixing simulations at 0600 UTC 28 January from the 6–10-km layer surrounding the area of upper-level height differences (green box in Fig. 12a).

The majority of parcels experiencing the most ascent in each swarm originate in the warm sector to the east of the storm center and rise to the north of the cyclone center (Figs. 14a,b), resembling the conceptual model of a warm conveyor belt in Schemm and Wernli (2014). A smaller subset of parcels

originate to the east of the North Carolina and Virginia coastline and ascend sharply to the 300-hPa level before transiting to the north of the cyclone, revealing a southern ascent pathway in both simulations. Interestingly, the more-mixing simulation generates more parcels in this southern pathway than the less-mixing simulation. We speculate that stronger PBL mixing reduces CIN and may have led to earlier triggering of convection in the more-mixing simulation similar to the process described in Hong et al. (2006). Aside from the southern ascent pathway differences, ascending parcels follow similar paths in both simulations; however, the ostensibly similar Lagrangian structures belie important differences in the properties of the ascending parcel swarms. Therefore, we compare the bulk characteristics of each trajectory swarm between the two simulations to investigate the source of the upper-level height differences seen in Fig. 12a.

Figures 15a–c depicts the pressure, temperature, and moisture content distributions of each simulation’s backward trajectory swarm through 24 h. Trajectories from the less-mixing simulation originate at higher pressures and ascend through a greater depth than the more-mixing simulation trajectories across the swarm distribution (Fig. 15a). This ascent is coincident with a larger potential temperature difference between trajectory origination and termination times in the less-mixing simulation (Fig. 15b), implying those parcels experienced stronger diabatic heating than those in the more-mixing run. Furthermore, the less-mixing trajectories originate with significantly higher water vapor content and terminate with roughly similar vapor content as the more-mixing trajectories (Fig. 15c). The larger deficit in specific humidity, along with the greater ascent and warmer termination temperatures, suggests

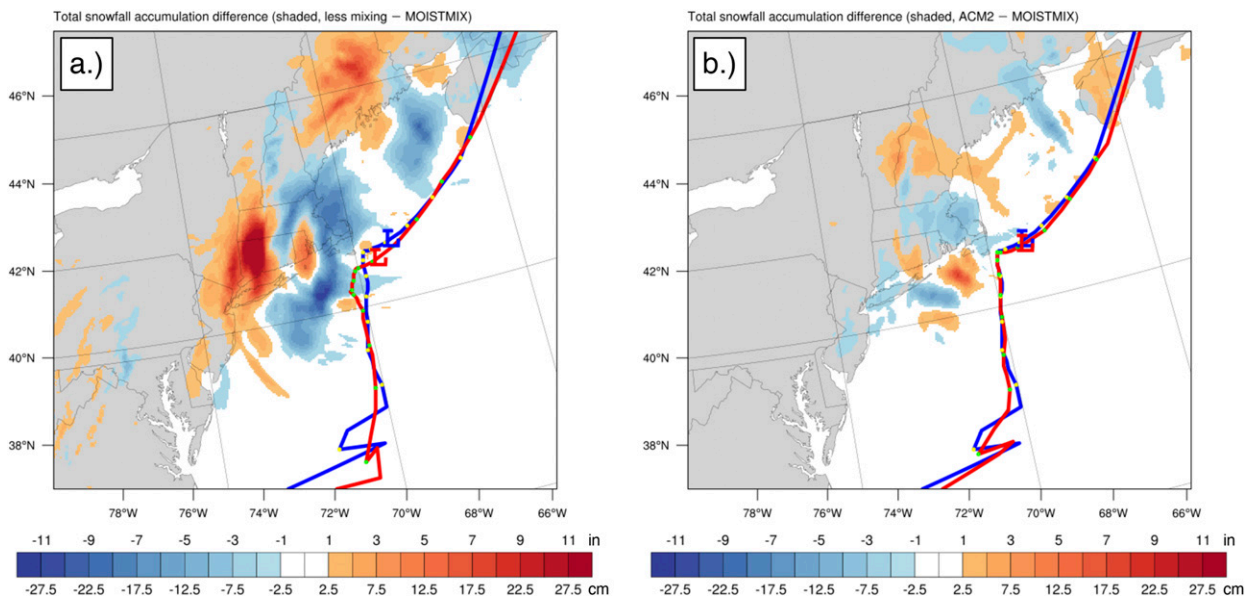


FIG. 11. (a) MSLP center tracks for the less-mixing (red) and MOISTMIX (blue) simulations and total snowfall accumulation difference (less mixing – MOISTMIX; cm, with inch scale also included). For each simulation, dots are 3-hourly surface cyclone center locations and L represents the surface low center location at 0600 UTC 28 Jan 2015. (b) As in (a), but for the ACM2 (red) and MOISTMIX [blue; the track is identical to that in (a)] simulations.

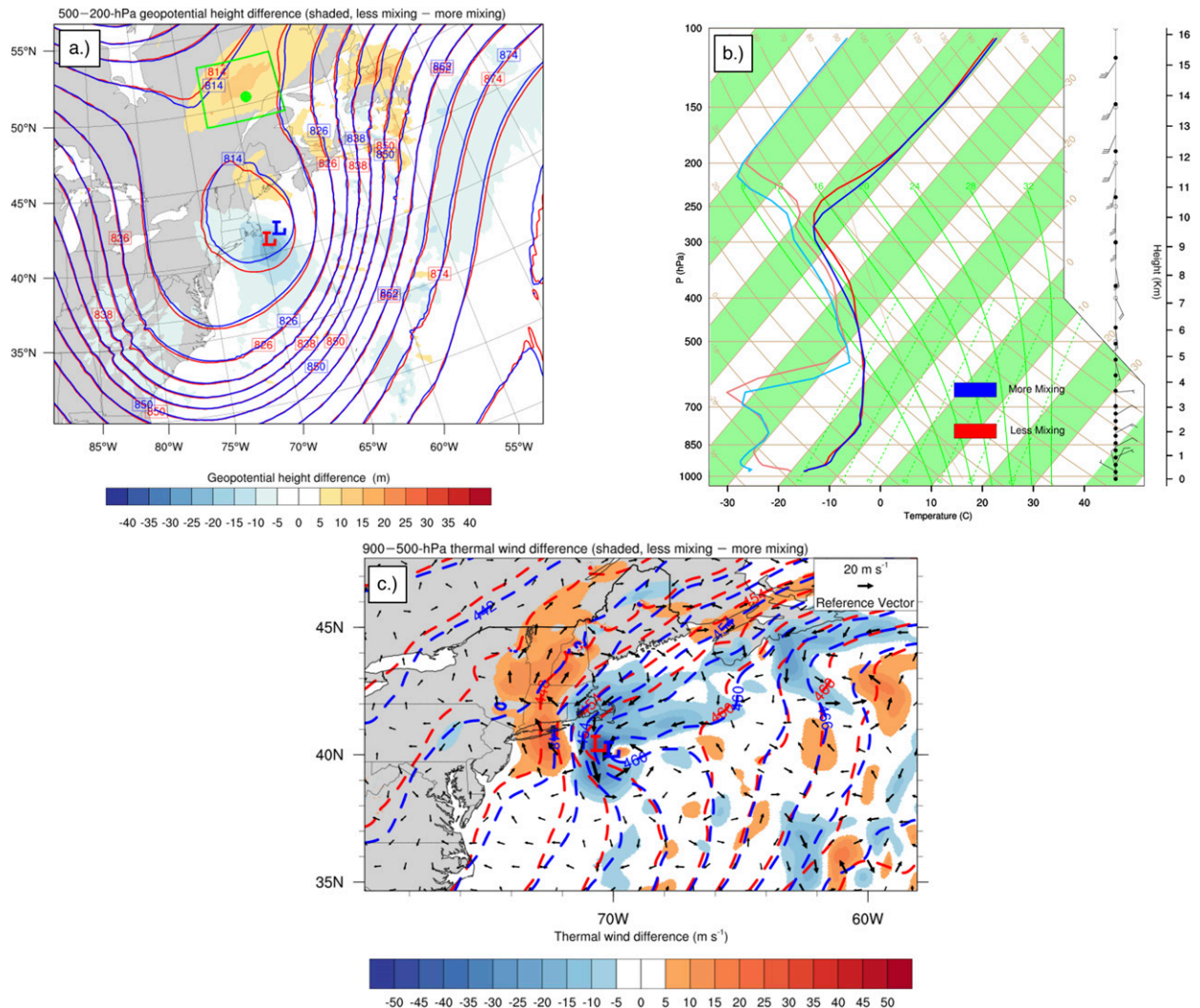


FIG. 12. (a) The 500–200-hPa geopotential heights (contours; dam) for the less-mixing (red) and more-mixing (blue) runs and the difference (less mixing – more mixing) of the 500–200-hPa geopotential height (shading; m) valid at 0600 UTC 28 Jan. The less- and more-mixing minimum MSLP locations are denoted with a red L and blue L, respectively. The green-bordered box outlines the starting location for the trajectory calculations in section 4. (b) Vertical profiles of temperature and dewpoint for the less-mixing (red) and more-mixing (blue) simulations at the green dot in (a), valid at 0600 UTC 28 Jan. (c) The 900–500-hPa thickness (dashed contours; dam) for the less-mixing (red) and more-mixing (blue) runs and the magnitude (shading) and vector difference (less mixing – more mixing; vectors) of 900–500-hPa thermal wind ( $\text{m s}^{-1}$ ) valid at 1800 UTC 27 Jan. Thickness fields are smoothed using a nine-point local smoother, run 150 times.

that the less-mixing simulation’s parcel trajectories undergo stronger condensational heating during their lifetimes, thereby promoting warmer temperatures aloft (Fig. 12b) and greater upper-tropospheric ridge building downstream of the surface cyclone (Fig. 12a). The more amplified flow pattern accompanies higher MUCAPE and greater low-level water vapor content values in the less-mixing run, contributing in a slower northeastward progression of the surface cyclone.

### 5. Discussion and summary

Several studies have demonstrated how boundary layer processes can exert a substantial influence on baroclinic

cyclone evolution. Specifically, the fluxes of heat and momentum from the surface impact the strength of Ekman pumping and the production of boundary layer PV, which can influence the system-scale circulation (Adamson et al. 2006; Beare 2007; Plant and Belcher 2007). However, previous studies of PBL processes within baroclinic cyclones have generally used dry, idealized model simulations. An important role for water substance can be anticipated from the tropical cyclone literature, which indicates PBL mixing can have a substantial impact on TC structure and evolution (Nolan et al. 2009; Kepert 2012; Bu et al. 2017). In particular, Bu et al. (2017) demonstrated the vertical mixing of water vapor may influence TC size via modification of outer-core convective activity.

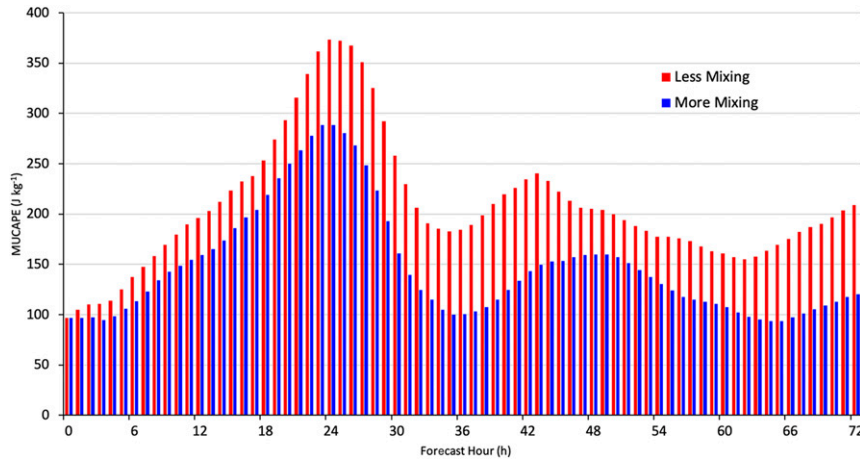


FIG. 13. Warm-sector area-averaged MUCAPE for the less-mixing (red) and more-mixing (blue) simulations.

This motivated a study concerning the sensitivity of moist baroclinic cyclone evolution to parameterized boundary layer mixing strength. Our principal finding is that variations in eddy diffusion within the PBL can modify cyclone evolution, particularly the propagation of the surface cyclone. The 26–29 January 2015 snowstorm, which dropped heavy snow across densely populated areas along the Northeast coastline and whose snowfall footprint was considerably dependent on cyclone track (Greybush et al. 2017), provides an example of how small changes in model physics can have substantial impacts on 2–3-day forecasts. By comparing simulations of this storm using the MYNN, YSU, and ACM2 PBL schemes, representing three approaches to handling the PBL mixing available in the

WRF Model, we determined that the choice of PBL scheme can influence sensible weather impacts of the baroclinic cyclone by altering precipitation patterns and surface cyclone movement.

Both YSU and ACM2 use  $K$ -profile assumptions that are sensitive to the choice of critical Richardson number. The schemes use different CRN values when the surface layer is determined to be unstable, reflecting disparate approaches to handling PBL-top entrainment. However, irrespective of the manner in which entrainment is treated, we demonstrated the variations between the YSU and ACM2 simulations with respect to snowfall footprint and surface cyclone movement could largely be reproduced by manipulating

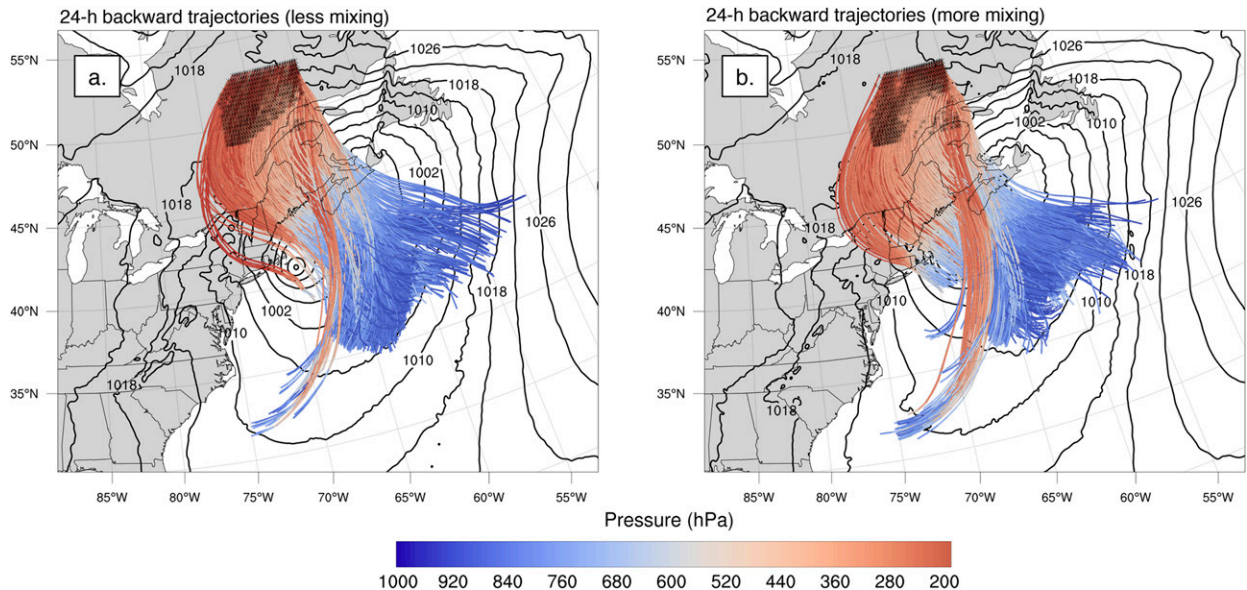


FIG. 14. MSLP (contours; hPa) and 24-h back trajectories (filled lines; hPa), initialized at 0600 UTC 28 Jan, for the (a) less-mixing and (b) more-mixing simulations. For clarity, only those trajectories within the top 25th percentile of all back trajectories, with respect to 24-h ascent, are shown.



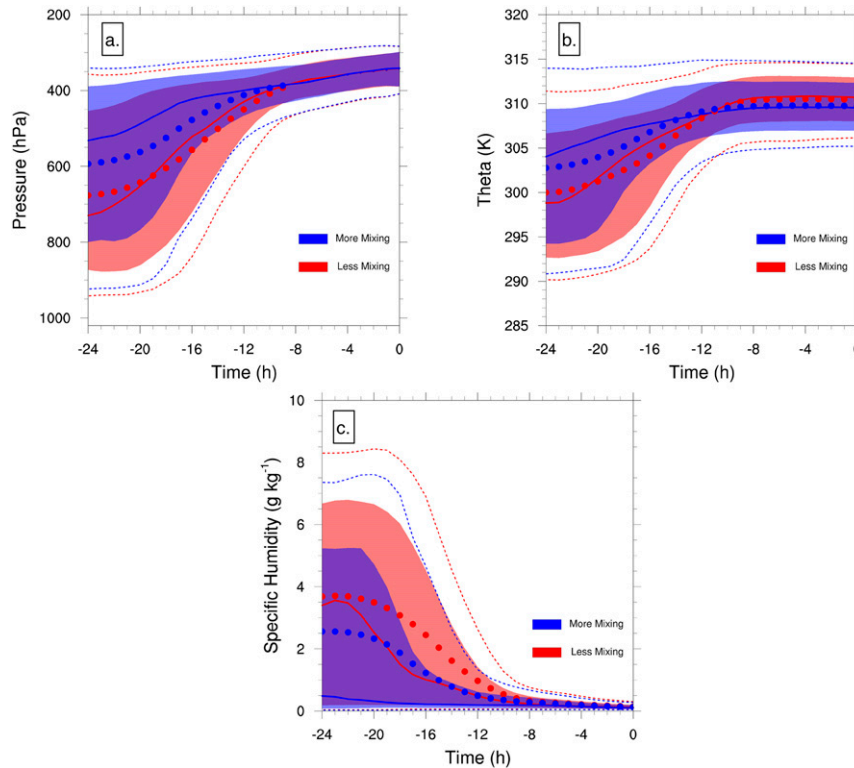


FIG. 15. Distributions of 24-h backward trajectories, ending at 0600 UTC 28 Jan, for the less-mixing (red) and more-mixing (blue) simulations for (a) pressure, (b) potential temperature, and (c) specific humidity. The distribution medians (solid lines), interquartile ranges (shading), upper and lower deciles (dashed lines), and distribution means (dots) are plotted. Large dots indicate distribution mean differences that are significant at the 99% confidence level using bootstrap resampling with replacement (10 000 generated samples and a sample population equaling the total number of trajectories in each distribution).

the CRN value within the YSU scheme itself to match that employed by ACM2.

Specifically, changing the unstable regime CRN from (the default) 0.00 (less mixing) to 0.25 (more mixing) in the YSU had a sizable impact on the magnitude and depth of the eddy diffusivity generated within the warm sector of the storm. Furthermore, lower CRN values consistently slowed the northeastward progression of the surface cyclone relative to the higher CRN runs, which impacts surface precipitation totals and type. Results from the SKEBS ensemble imply random chance is unlikely to cause these shifts and the special MOISTMIX experiment that limited CRN-associated mixing changes to water species alone demonstrates the primary role of water vapor in modulating the cyclone motion.

The mechanism by which changes in eddy mixing of moisture impact cyclone propagation is evidenced by differences in downstream ridging ahead of the surface cyclone between the less-mixing/more-mixing runs. Simulations with less mixing had stronger ridge building attendant with warmer temperatures in the middle and upper troposphere, amplifying the upper-level flow pattern and slowing the northeastward movement of the system. Reduced values of eddy diffusivity and a shallower PBL contribute to weaker entrainment

of drier, free-tropospheric air into the PBL, less ventilation of near-surface moisture out of the PBL, and preservation of higher PBL moisture values within several hundred meters of the surface. This increased moisture content is consistent with higher MUCAPE in the less-mixing simulation and implies more vigorous upward vertical motion transpires when boundary layer parcels are lifted, leading to more condensational heating and contributing to further ridge building. Backward trajectory analysis suggests the strongest ascent occurs within the warm conveyor belt as parcels are lifted over the warm front. Trajectories terminating in the downstream ridge undergo greater ascent and diabatic heating in the less-mixing case, as a result of originating with more moisture and at higher pressures in the troposphere, consistent with the results of Schäfler and Harnisch (2015) who found drier inflow regions led to lower outflow heights for warm conveyor belt parcels. The enhanced heating both weakens the thermal wind over the less-mixing cyclone and promotes a stronger upper-tropospheric downstream ridge, which combine to inhibit the northeastward propagation of the less-mixing surface cyclone.

The results of this study are intended to demonstrate both the sensitivity of baroclinic cyclones to PBL mixing strength

and the predominant pathway through which that sensitivity manifests itself. A variety of PBL parameterization schemes exist, with little consensus with regard to which scheme produces the most realistic mixing in the boundary layer. The sensitivity to PBL mixing exhibited by the baroclinic cyclone simulated herein, as well as other phenomena such as tropical cyclones and severe convection discussed in previous studies, motivates future work to better represent uncertainty surrounding PBL mixing strength. Stochastic perturbations of parameters (SPP), such as the CRN in the YSU scheme or other parameters governing vertical mixing that are not well constrained, may be considered as a strategy to address the uncertainty in PBL mixing within ensemble weather prediction systems.

Several studies have sought to represent the uncertainties in assumptions within physics parameterization schemes, including PBL schemes, using the SPP approach (Ollinaho et al. 2017; Jankov et al. 2017, 2018). Jankov et al. (2017, 2018) evaluated 24-h WRF forecasts using various stochastic perturbation strategies and found SPP can improve model performance, particularly when combined with other perturbation strategies such as SKEBS and stochastic perturbations of physics tendencies (SPPT). Ollinaho et al. (2017) evaluated an SPP scheme against an SPPT scheme within the ECMWF IFS over 15-day forecast periods and found improved 2-m temperature forecasts over the first couple of days. While only one of these studies limited their SPP strategy to the PBL scheme (Jankov et al. 2018), their collective results suggest SPP schemes can improve model spread, particularly near the surface where SPPT schemes are commonly tapered to zero in order to avoid numerical instabilities (Ollinaho et al. 2017). The present work builds on previous research and hypothesizes a pathway through which perturbations of PBL mixing, specifically mixing of water vapor, may project to larger scales. It is anticipated that understanding the pathways through which physics perturbations may grow upscale and impact synoptic weather features may lead to more informed and targeted applications of physics perturbation methods within numerical weather prediction systems.

*Acknowledgments.* The authors thank three anonymous reviewers for their very constructive comments on this paper. This research was funded by the U.S. Department of Defense (DoD) through the National Defense Science and Engineering Graduate Fellowship (NDSEG) Program. The ERAI data were provided by the Research Data Archive (RDA) of the Computational and Information Systems Laboratory at the National Center for Atmospheric Research. NCAR is supported by grants from the National Science Foundation (NSF). Constructive comments from Lance Bosart further enhanced this work. This research was also supported by NSF Grant AGS1921546.

*Data availability statement.* ERA-Interim data used in this study are available at the NCAR Research Data Archive (<https://doi.org/10.5065/D6CR5RD9>). The WRF Model source code is available online (<https://github.com/wrf-model/WRF>). WRF simulation data are archived at the University at Albany

and will be made available upon request. The LAGRANTO software used in this study is available online (<http://iacweb.ethz.ch/staff/sprenger/lagranto/download.html>).

## REFERENCES

- Adamson, D. S., S. E. Belcher, B. J. Hoskins, and R. S. Plant, 2006: Boundary-layer friction in midlatitude cyclones. *Quart. J. Roy. Meteor. Soc.*, **132**, 101–124, <https://doi.org/10.1256/qj.04.145>.
- Ahmadi-Givi, F., G. C. Graig, and R. S. Plant, 2004: The dynamics of a midlatitude cyclone with very strong latent-heat release. *Quart. J. Roy. Meteor. Soc.*, **130**, 295–323, <https://doi.org/10.1256/qj.02.226>.
- Babay, E., 2015: Meteorologists apologize for busted forecast. *The Philadelphia Inquirer*, 27 January 2015, [https://www.inquirer.com/philly/news/Meteorologists\\_apologize\\_for\\_busted\\_forecast.html](https://www.inquirer.com/philly/news/Meteorologists_apologize_for_busted_forecast.html).
- Baxter, M. A., C. E. Graves, and J. T. Moore, 2005: A climatology of snow-to-liquid ratio for the contiguous United States. *Wea. Forecasting*, **20**, 729–744, <https://doi.org/10.1175/WAF856.1>.
- Beare, R. J., 2007: Boundary layer mechanisms in extratropical cyclones. *Quart. J. Roy. Meteor. Soc.*, **133**, 503–515, <https://doi.org/10.1002/qj.30>.
- Benjamin, S. G., and Coauthors, 2016: A North American hourly assimilation and model forecast cycle: The Rapid Refresh. *Mon. Wea. Rev.*, **144**, 1669–1694, <https://doi.org/10.1175/MWR-D-15-0242.1>.
- Berner, J., S.-Y. Ha, J. P. Hacker, A. Fournier, and C. Snyder, 2011: Model uncertainty in a mesoscale ensemble prediction system: Stochastic versus multiphysics representations. *Mon. Wea. Rev.*, **139**, 1972–1995, <https://doi.org/10.1175/2010MWR3595.1>.
- Binder, H., M. Boettcher, H. Joos, and H. Wernli, 2016: The role of warm conveyor belts for the intensification of extratropical cyclones in Northern Hemisphere winter. *J. Atmos. Sci.*, **73**, 3997–4020, <https://doi.org/10.1175/JAS-D-15-0302.1>.
- Boutle, I., R. Beare, S. E. Belcher, A. Brown, and R. Plant, 2009: The moist boundary layer under a mid-latitude weather system. *Bound.-Layer Meteor.*, **134**, 367–386, <https://doi.org/10.1007/s10546-009-9452-9>.
- , S. E. Belcher, and R. S. Plant, 2014: Friction in mid-latitude cyclones: An Ekman-PV mechanism. *Atmos. Sci. Lett.*, **16**, 103–109, <https://doi.org/10.1002/asl2.526>.
- Brennan, M. J., and G. M. Lackmann, 2005: The influence of incipient latent heat release on the precipitation distribution of the 24–25 January 2000 U.S. East Coast cyclone. *Mon. Wea. Rev.*, **133**, 1913–1937, <https://doi.org/10.1175/MWR2959.1>.
- Bu, Y. P., R. G. Fovell, and K. L. Corbosiero, 2017: The influences of boundary layer mixing and cloud-radiative forcing on tropical cyclone size. *J. Atmos. Sci.*, **74**, 1273–1292, <https://doi.org/10.1175/JAS-D-16-0231.1>.
- Carlson, T. N., 1980: Airflow through midlatitude cyclones and the comma cloud pattern. *Mon. Wea. Rev.*, **108**, 1498–1509, [https://doi.org/10.1175/1520-0493\(1980\)108<1498:ATMCAT>2.0.CO;2](https://doi.org/10.1175/1520-0493(1980)108<1498:ATMCAT>2.0.CO;2).
- Cohen, A. E., S. M. Cavallo, M. C. Coniglio, and H. E. Brooks, 2015: A review of planetary boundary layer parameterization schemes and their sensitivity in simulating southeastern U.S. cold season severe weather environments. *Wea. Forecasting*, **30**, 591–612, <https://doi.org/10.1175/WAF-D-14-00105.1>.
- , —, —, —, and I. L. Jirak, 2017: Evaluation of multiple planetary boundary layer parameterization schemes in Southeast U.S. cold season severe thunderstorm environments. *Wea. Forecasting*, **32**, 1857–1884, <https://doi.org/10.1175/WAF-D-16-0193.1>.
- Davis, C. A., 1992: A potential-vorticity diagnosis of the importance of initial structure and condensational heating in

- observed extratropical cyclogenesis. *Mon. Wea. Rev.*, **120**, 2409–2428, [https://doi.org/10.1175/1520-0493\(1992\)120<2409:APVDOT>2.0.CO;2](https://doi.org/10.1175/1520-0493(1992)120<2409:APVDOT>2.0.CO;2).
- , and K. A. Emanuel, 1988: Observational evidence for the influence of surface heat fluxes on rapid maritime cyclogenesis. *Mon. Wea. Rev.*, **116**, 2649–2659, [https://doi.org/10.1175/1520-0493\(1988\)116<2649:OEFTIO>2.0.CO;2](https://doi.org/10.1175/1520-0493(1988)116<2649:OEFTIO>2.0.CO;2).
- , M. T. Stoelinga, and Y.-H. Kuo, 1993: The integrated effect of condensation in numerical simulations of extratropical cyclogenesis. *Mon. Wea. Rev.*, **121**, 2309–2330, [https://doi.org/10.1175/1520-0493\(1993\)121<2309:TIEOCI>2.0.CO;2](https://doi.org/10.1175/1520-0493(1993)121<2309:TIEOCI>2.0.CO;2).
- Dee, D. P., and Coauthors, 2011: The ERA-Interim reanalysis: Configuration and performance of the data assimilation system. *Quart. J. Roy. Meteor. Soc.*, **137**, 553–597, <https://doi.org/10.1002/qj.828>.
- Duda, J. D., X. Wang, F. Kong, M. Xue, and J. Berner, 2016: Impact of a stochastic kinetic energy backscatter scheme on warm season convection-allowing ensemble forecasts. *Mon. Wea. Rev.*, **144**, 1887–1908, <https://doi.org/10.1175/MWR-D-15-0092.1>.
- Ek, M. B., K. E. Mitchell, Y. Lin, E. Rogers, P. Grunmann, V. Koren, G. Gayno, and J. D. Tarpley, 2003: Implementation of Noah land surface model advances in the National Centers for Environmental Prediction operational mesoscale Eta model. *J. Geophys. Res.*, **108**, 8851, <https://doi.org/10.1029/2002JD003296>.
- European Centre for Medium-Range Weather Forecasts, 2009: ERA-Interim Project. Research Data Archive at the National Center for Atmospheric Research, Computational and Information Systems Laboratory, Boulder CO, accessed 21 April 2017, <https://doi.org/10.5065/D6CR5RD9>.
- Greybush, S. J., S. Saslo, and R. Grumm, 2017: Assessing the ensemble predictability of precipitation forecasts for the January 2015 and 2016 East Coast winter storms. *Wea. Forecasting*, **32**, 1057–1078, <https://doi.org/10.1175/WAF-D-16-0153.1>.
- Holtslag, A. A. M., and B. A. Boville, 1993: Local versus nonlocal boundary-layer diffusion in a global climate model. *J. Climate*, **6**, 1825–1842, [https://doi.org/10.1175/1520-0442\(1993\)006<1825:LVNBLD>2.0.CO;2](https://doi.org/10.1175/1520-0442(1993)006<1825:LVNBLD>2.0.CO;2).
- Hong, S.-Y., 2010: A new stable boundary-layer mixing scheme and its impact on the simulated East Asian summer monsoon. *Quart. J. Roy. Meteor. Soc.*, **136**, 1481–1496, <https://doi.org/10.1002/qj.665>.
- , and H.-L. Pan, 1996: Nonlocal boundary layer vertical diffusion in a medium-range forecast model. *Mon. Wea. Rev.*, **124**, 2322–2339, [https://doi.org/10.1175/1520-0493\(1996\)124<2322:NBLVDI>2.0.CO;2](https://doi.org/10.1175/1520-0493(1996)124<2322:NBLVDI>2.0.CO;2).
- , Y. Noh, and J. Dudhia, 2006: A new vertical diffusion package with an explicit treatment of entrainment processes. *Mon. Wea. Rev.*, **134**, 2318–2341, <https://doi.org/10.1175/MWR3199.1>.
- Jankov, I., and Coauthors, 2017: A performance comparison between multiphysics and stochastic approaches within a North American RAP ensemble. *Mon. Wea. Rev.*, **145**, 1161–1179, <https://doi.org/10.1175/MWR-D-16-0160.1>.
- , J. Beck, J. Wolff, M. Harrold, J. B. Olson, T. Smirnova, C. Alexander, and J. Berner, 2018: Stochastically perturbed parameterizations in an HRRR-based ensemble. *Mon. Wea. Rev.*, **147**, 153–173, <https://doi.org/10.1175/MWR-D-18-0092.1>.
- Jiménez, P. A., J. Dudhia, J. F. González-Rouco, J. Navarro, J. P. Montávez, and E. García-Bustamante, 2012: A revised scheme for the WRF surface layer formulation. *Mon. Wea. Rev.*, **140**, 898–918, <https://doi.org/10.1175/MWR-D-11-00056.1>.
- Joos, H., and H. Wernli, 2012: Influence of microphysical processes on the potential vorticity development in a warm conveyor belt: A case-study with the limited-area model COSMO. *Quart. J. Roy. Meteor. Soc.*, **138**, 407–418, <https://doi.org/10.1002/qj.934>.
- Keper, J. D., 2012: Choosing a boundary layer parameterization for tropical cyclone modeling. *Mon. Wea. Rev.*, **140**, 1427–1445, <https://doi.org/10.1175/MWR-D-11-00217.1>.
- Kuo, Y.-H., M. A. Shapiro, and E. G. Donall, 1990: The interaction between baroclinic and diabatic processes in a numerical simulation of a rapidly intensifying extratropical marine cyclone. *Mon. Wea. Rev.*, **119**, 368–384, [https://doi.org/10.1175/1520-0493\(1991\)119<0368:TIBBAD>2.0.CO;2](https://doi.org/10.1175/1520-0493(1991)119<0368:TIBBAD>2.0.CO;2).
- Minder, J. R., W. M. Bartolini, C. Spence, N. R. Hedstrom, P. D. Blanken, and J. D. Lenters, 2020: Characterizing and constraining uncertainty associated with surface and boundary layer turbulent fluxes in simulations of lake-effect snowfall. *Wea. Forecasting*, **35**, 467–488, <https://doi.org/10.1175/WAF-D-19-0153.1>.
- Nakanishi, M., and H. Niino, 2009: Development of an improved turbulence closure model for the atmospheric boundary layer. *J. Meteor. Soc. Japan*, **87**, 895–912, <https://doi.org/10.2151/jmsj.87.895>.
- National Center for Atmospheric Research, 2015: User's guide for the Advanced Research WRF (ARW) modelling system, version 3. National Center for Atmospheric Research, accessed 19 January 2016, [https://www2.mmm.ucar.edu/wrf/users/docs/user\\_guide\\_V3.7/contents.html](https://www2.mmm.ucar.edu/wrf/users/docs/user_guide_V3.7/contents.html).
- Nolan, D. S., J. A. Zhang, and D. P. Stern, 2009: Evaluation of planetary boundary layer parameterizations in tropical cyclones by comparison of in situ observations and high-resolution simulations of Hurricane Isabel (2003). Part I: Initialization, maximum winds, and the outer-core boundary layer. *Mon. Wea. Rev.*, **137**, 3651–3674, <https://doi.org/10.1175/2009MWR2785.1>.
- Ollinaho, P., and Coauthors, 2017: Towards process-level representation of model uncertainties: Stochastically perturbed parameterizations in the ECMWF ensemble. *Quart. J. Roy. Meteor. Soc.*, **143**, 408–422, <https://doi.org/10.1002/qj.2931>.
- Olson, J. B., J. S. Kenyon, W. A. Angevine, J. M. Brown, M. Pagowski, and K. Sušelj, 2019: A description of the MYNN-EDMF scheme and the coupling to other components in WRF-ARW. NOAA Tech. Memo. OAR GSD-61, 42 pp., <https://doi.org/10.25923/n9wm-be49>.
- Plant, R. S., and S. E. Belcher, 2007: Numerical simulation of baroclinic waves with a parameterized boundary layer. *J. Atmos. Sci.*, **64**, 4383–4399, <https://doi.org/10.1175/2007JAS2269.1>.
- Pleim, J. E., 2007: A combined local and nonlocal closure model for the atmospheric boundary layer. Part I: Model description and testing. *J. Appl. Meteor. Climatol.*, **46**, 1383–1395, <https://doi.org/10.1175/JAM2539.1>.
- Reed, R. J., M. D. Albright, A. J. Sammons, and P. Undén, 1988: The role of latent heat release in explosive cyclogenesis: Three examples based on ECMWF operational forecasts. *Wea. Forecasting*, **3**, 217–229, [https://doi.org/10.1175/1520-0434\(1988\)003<0217:TROLHR>2.0.CO;2](https://doi.org/10.1175/1520-0434(1988)003<0217:TROLHR>2.0.CO;2).
- Schäfler, A., and F. Harnisch, 2015: Impact of the inflow moisture on the evolution of a warm conveyor belt. *Quart. J. Roy. Meteor. Soc.*, **141**, 299–310, <https://doi.org/10.1002/qj.2360>.
- Schemm, S., and H. Wernli, 2014: The linkage between the warm and the cold conveyor belts in an idealized extratropical cyclone. *J. Atmos. Sci.*, **71**, 1443–1459, <https://doi.org/10.1175/JAS-D-13-0177.1>.



- Sprenger, M., and H. Wernli, 2015: The LAGRANTO Lagrangian analysis tool—version 2.0. *Geosci. Model Dev.*, **8**, 2569–2586, <https://doi.org/10.5194/gmd-8-2569-2015>.
- Stoelinga, M. T., 1996: A potential vorticity-based study of the role of diabatic heating and friction in a numerically simulated baroclinic cyclone. *Mon. Wea. Rev.*, **124**, 849–874, [https://doi.org/10.1175/1520-0493\(1996\)124<0849:APVBSO>2.0.CO;2](https://doi.org/10.1175/1520-0493(1996)124<0849:APVBSO>2.0.CO;2).
- Sutcliffe, R. C., 1947: A contribution to the problem of development. *Quart. J. Roy. Meteor. Soc.*, **73**, 370–383, <https://doi.org/10.1002/qj.49707331710>.
- Trenberth, K. E., 1978: On the interpretation of the diagnostic quasi-geostrophic omega equation. *Mon. Wea. Rev.*, **106**, 131–137, [https://doi.org/10.1175/1520-0493\(1978\)106<0131:OTIOTD>2.0.CO;2](https://doi.org/10.1175/1520-0493(1978)106<0131:OTIOTD>2.0.CO;2).
- Valdes, P. J., and B. J. Hoskins, 1988: Baroclinic instability of the zonally averaged flow with boundary layer damping. *J. Atmos. Sci.*, **45**, 1584–1593, [https://doi.org/10.1175/1520-0469\(1988\)045<1584:BIOTZA>2.0.CO;2](https://doi.org/10.1175/1520-0469(1988)045<1584:BIOTZA>2.0.CO;2).
- Wernli, B. H., and H. C. Davies, 1997: A Lagrangian-based analysis of extratropical cyclones. I: The method and some applications. *Quart. J. Roy. Meteor. Soc.*, **123**, 467–489, <https://doi.org/10.1002/qj.49712353811>.
- Whitaker, J. S., and C. A. Davis, 1994: Cyclogenesis in a saturated environment. *J. Atmos. Sci.*, **51**, 889–908, [https://doi.org/10.1175/1520-0469\(1994\)051<0889:CIASE>2.0.CO;2](https://doi.org/10.1175/1520-0469(1994)051<0889:CIASE>2.0.CO;2).